Optimal Design and Control of an Aerial Manipulator with Elastic Suspension Using Unidirectional Thrusters

Miguel Arpa Perozo, Jean Dussine, Arda Yigit, Loïc Cuvillon, Sylvain Durand, Jacques Gangloff

Optimal Design and Control of an Aerial Manipulator with Elastic Suspension Using Unidirectional Thrusters

Miguel Arpa Perozo, Jean Dussine, Arda Yiğit, Loïc Cuvillon, Sylvain Durand and Jacques Gangloff

***Abstract*— Aerial Manipulators with Elastic Suspension (AMES) may be seen as a hybrid robot mixing properties of classical Aerial Manipulators (AMs) and Cable-Driven Parallel Robots (CDPRs). The optimal design and control of an AMES using unidirectional thrusters are considered in this paper. To maximize the workspace, an optimization algorithm is proposed. The position and orientation of the thrusters are optimized by adapting methods borrowed from both the AM and CDPR communities. The resulting design is used to build a prototype. Preliminary experimentations are carried out to validate the theoretical workspace and assess the trajectory tracking performance of this AMES. Experiments highlight the significant improvements with respect to a previous suboptimal prototype.**

I. Introduction

Cable-Driven Parallel Robots (CDPRs) and Aerial Manipulators (AMs) are cost-effective robots that can perform fast dexterous tasks over a large workspace. They are widely studied due to various potential applications, provided some intrinsic limitations can be corrected (e.g., accuracy).

Most optimal AM designs seek to i) have an omnidirectional structure with six decoupled degrees of freedom (DoFs) in order to be used for complex manipulation tasks [1], [2], ii) maximize the set of allowed wrench the AM can generate [3]. Orientation invariance in the design of the AM is also often sought. For example, the optimization of the ODAR robot [4] ensures that the robot can carry its own weight regarding its orientation. Similarly, it is possible to take advantage of mechanical symmetries in order to have an AM inertia tensor multiple of the identity matrix, making the wrench generation invariant with respect to (w.r.t) the drone orientation [5]. Another common feature is the use of bidirectional propellers. Standard drone brushless motor drivers, or electronic speed controllers (ESCs), are not equipped with position sensors, so they rely on the back electromotive force to estimate the rotor position. When the rotor has a low rotational speed (e.g., during a thrust inversion phase) the electromotive force can not be measured introducing a dead zone in the control of the AM. To bypass this problem, a theory was developed in order to optimally design omnidirectional aerial vehicles using unidirectional thrusters, called *omniplus* [6]. Examples of existing prototypes based on this design may be found in the literature [7], [8].

This work was supported by the e-VISER project funded by the French National Research Agency (ANR-17-CE33-0008).

The authors are with ICube Laboratory (UMR CNRS 7357), Strasbourg University, INSA Strasbourg, France email: {marpaperozo, arda.yigit, l.cuvillon, sdurand, jacques.gangloff}@unistra.fr

Like unidirectional thrusters, cables in CDPRs can only apply a unidirectional force to a platform. Hence, the design of AMs using unidirectional thrusters can benefit from the design strategies already developed in the CDPR community (see section IV). Several performance indices adapted to unidirectional actuators have already been developed [9], [10]. Optimal design of CDPRs has already been extensively studied over the last two decades, with the earliest studies in [11]. A great variety of design strategies are used in the CDPR community. A *design-to-task* approach is developed in [12] to choose the fastest robot for a given trajectory. The stiffness and dexterity of a planar CDPR are optimized in [13]. In [14], the maximum cable tension over the workspace (directly linked to the robot cost) is minimized. Both the workspace and dexterity of the robot are optimized in [15]. Finally, a multi-criteria optimization framework for parallel manipulators is developed in [16].

Nevertheless, CDPRs and AMs have some intrinsic limitations: (i) non-tethered AMs have limited flight time, (ii) the control of CDPRs can be challenging (complex workspaces, handling of redundant cable tensions, etc). In order to address some of those limitations, our team previously introduced the concept of Aerial Manipulator with Elastic Suspension (AMES) [17]. A prototype was manufactured, called *dextAIR* for *dexterous aerial manipulator*. The dextAIR concept may be seen as a simplified cable robot using only one elastic link (spring), where the end effector is an omnidirectional aerial vehicle. The spring compensates for the gravity, thus providing more autonomy to the AM while preserving its six DoFs. The spring has a low-stiffness to increase the workspace of the AM around its equilibrium point. Alternatively, the cable-Suspended Aerial Manipulator (SAM) [7] uses a redundant actuation with non-elastic cables and winches besides propellers to control the AM carrying a 7-DoF robotic arm.

The first version of the dextAIR [17] had an important limiting factor: the distance between the cable anchoring point and the center of mass of the robot creates a moment that reduces significantly the workspace. Moreover, to cope with the issue of bidirectional thrusters, the previous prototype made use of propulsion units using a pair of coaxial motors, increasing the mechanical complexity of the system. In the present paper, a new stochastic method that takes into account those limitations and that maximizes the AMES workspace is proposed by generating several omniplus designs and selecting the one with the largest workspace. Based on techniques from the CDPR community, we compute the *wrench-feasible workspace* using interval analysis in order

to assess the optimal structure. Finally, a prototype is built and its workspace and trajectory tracking performance are experimentally tested using a nonlinear model-based control law.

II. Model

A. System Parametrization and Notations

Let $\mathbf{u}$ and $\mathbf{v}$ be vectors and $\mathscr{F}_q$ a reference frame. The projection of $\mathbf{v}$ in $\mathscr{F}_q$ is written ${}^q\mathbf{v}$. The cross product of ${}^q\mathbf{u}$ and ${}^q\mathbf{v}$ is denoted ${}^q\mathbf{u}\times{}^q\mathbf{v}$ and $[\cdot]_\times$ is the cross product matrix such that ${}^q\mathbf{u}\times{}^q\mathbf{v}=[{}^q\mathbf{u}]_\times{}^q\mathbf{v}$. The identity matrix is noted $\mathbf{I}_j\in\mathbb{R}^{j\times j}$ and the matrix containing only zeros $\mathbf{0}_j\in\mathbb{R}^{j\times j}$.

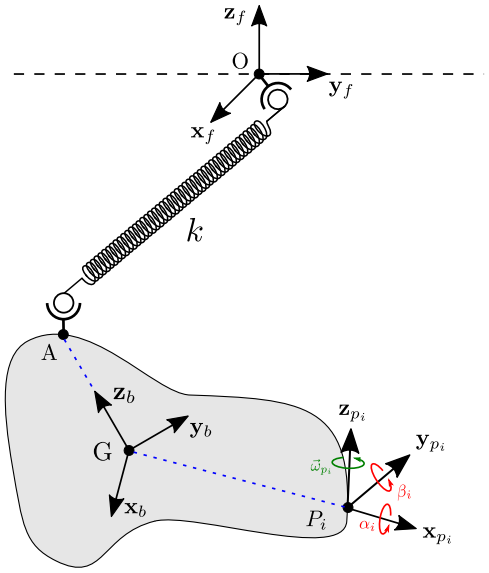

Fig. 1: Generic AMES model parameters.

Frames and model parameters are shown in Fig. 1. The mass of the spring is considered negligible. Let us consider an inertial frame $\mathscr{F}_f=\{O,\mathbf{x}_f,\mathbf{y}_f,\mathbf{z}_f\}$, and a body frame attached to the center of mass (CoM) G of the AMES $\mathscr{F}_b=\{G,\mathbf{x}_b,\mathbf{y}_b,\mathbf{z}_b\}$. The rotation matrix $\mathbf{R}_{fb}\in SO(3)$ describes the orientation of $\mathscr{F}_b$ w.r.t $\mathscr{F}_f$.

The aerial wrench generator (AWG) is considered to have n propellers. The frame of the i-th propeller is attached to its center P_i such that: $\mathscr{F}_{p_i}=\{P_i,\mathbf{x}_{p_i},\mathbf{y}_{p_i},\mathbf{z}_{p_i}\}$, where $\mathbf{z}_{p_i}$ corresponds to the direction of the generated thrust. The orientation of the i-th propeller thrust $\mathbf{z}_{p_i}$ is determined by two rotations along mobile axes $(x-y)$: α_i and β_i. The rotation matrix $\mathbf{R}_{bp_i}\in SO(3)$ describes the orientation of the i-th propeller w.r.t the body frame $\mathscr{F}_b$. The mobile anchoring point of the spring is noted A. The position vector of the CoM G w.r.t $\mathscr{F}_f$ is $\mathbf{p}$. The force and moment at the CoM applied by the spring on the AWG are respectively $\mathbf{F}_s$ and $\mathbf{N}_s$:

$$\mathbf{F}_s=k\left(l_0-\|\mathbf{OA}\|\right)\frac{\mathbf{OA}}{\|\mathbf{OA}\|} \tag{1}$$

$$\mathbf{N}_s=\|\mathbf{GA}\|\,\mathbf{z}_b\times\mathbf{F}_s \tag{2}$$

where l_0 is the free length of the spring and k its stiffness.

B. Robot Dynamics

Let $\mathbf{X}=(\mathbf{p}^T\ \boldsymbol{\eta}^T)^T$ be the pose coordinates of the AMES w.r.t. $\mathscr{F}_f$, with $\boldsymbol{\eta}$ a set of Euler angles. The dynamic model of the AMES was developed in [17] and is given as follows in the Cartesian-space canonical formulation:

$$\mathbf{M}(\mathbf{X})\ddot{\mathbf{X}}+\mathbf{C}(\mathbf{X},\dot{\mathbf{X}})\dot{\mathbf{X}}+\mathbf{G}(\mathbf{X})=\tilde{\mathbf{W}}(\mathbf{X})\mathbf{w_2} \tag{3}$$

with

$$\begin{cases}\mathbf{M}(\mathbf{X}) &= \begin{pmatrix}m\mathbf{I}_3 & \mathbf{0}_3\\ \mathbf{0}_3 & \mathbf{S}^{Tb}\mathbf{J}\mathbf{S}\end{pmatrix}\\ \mathbf{C}(\mathbf{X},\dot{\mathbf{X}}) &= \begin{pmatrix}\mathbf{0}_3 & \mathbf{0}_3\\ \mathbf{0}_3 & \mathbf{S}^T({}^b\mathbf{J}\dot{\mathbf{S}}+[\mathbf{S}\dot{\boldsymbol{\eta}}]_\times{}^b\mathbf{J}\mathbf{S})\end{pmatrix}\\ \mathbf{G}(\mathbf{X}) &= \begin{pmatrix}-m{}^f\mathbf{g}-{}^f\mathbf{F_s}\\ -\mathbf{S}^{Tb}\mathbf{N_s}\end{pmatrix}\\ \tilde{\mathbf{W}}(\mathbf{X}) &= \begin{pmatrix}\mathbf{R_{fb}} & \mathbf{0}_3\\ \mathbf{0}_3 & \mathbf{S}^T\end{pmatrix}\mathbf{W}_t\end{cases}$$

where $m>0$ is the total mass of the platform, ${}^b\mathbf{J}\in\mathbb{R}^{3\times3}$ its inertia tensor at the CoM expressed in $\mathscr{F}_b$, ${}^f\mathbf{g}\in\mathbb{R}^3$ the gravity acceleration, ${}^f\mathbf{F}_s\in\mathbb{R}^3$ the force of the elastic link on the AMES and ${}^b\mathbf{N}_s\in\mathbb{R}^3$ the associated torque at the CoM. The matrix $\mathbf{S}(\boldsymbol{\eta})\in\mathbb{R}^{3\times3}$ is the analytical Jacobian, mapping the time derivative of $\boldsymbol{\eta}$ to the angular velocity expressed in the body frame. The *wrench* or *allocation* matrix $\mathbf{W}_t\in\mathbb{R}^{6\times n}$ maps the propeller thrusts $\mathbf{u}\in\mathbb{R}^n$ to the wrench applied to the platform at the CoM:

$$\mathbf{W}_t=\begin{pmatrix}\cdots & \mathbf{z}_{p_i} & \cdots\\ \cdots & \mathbf{GP}_i\times\mathbf{z}_{p_i} & \cdots\end{pmatrix} \tag{4}$$

$$\begin{pmatrix}\mathbf{F}_b\\ \mathbf{N}_b\end{pmatrix}=\mathbf{W}_t\cdot\mathbf{u} \tag{5}$$

with $\mathbf{F}_b$ and $\mathbf{N}_b$ the total force and moment generated by the propellers at the CoM. The thrust coefficient a (in $[\mathrm{N\,rad^{-2}\,s^2}]$), links the thrust generated by the propellers to the square of their rotational speed $\omega_{p_i}\in\mathbb{R}$. The column matrix $\mathbf{w}_2=(\cdots\ \omega_i|\omega_i|\ \cdots)^T$ contains the signed squared propeller rotational speed of the n propellers.

C. Static Analysis

We define the set of *allowed propeller thrusts* $[\mathbf{u}]$ as:

$$[\mathbf{u}]=\left\{\mathbf{u}\mid u_i\in\left[\underline{u_i},\,\overline{u_i}\right],\ 1\le i\le n\right\} \tag{6}$$

where $\underline{u_i}$ and $\overline{u_i}$ correspond to the minimum and maximum thrusts that the i-th propeller can generate.

Definition 1: A given pose $\mathbf{X}$ is said to be reachable if the propellers can compensate for the external forces applied to the platform:

$$\exists\,\mathbf{u}\in[\mathbf{u}]\mid\mathbf{W}_t\mathbf{u}=\begin{pmatrix}\mathbf{F}_s(\mathbf{X})+\mathbf{g}(\mathbf{X})\\ \mathbf{N}_s(\mathbf{X})\end{pmatrix} \tag{7}$$

The *reachable workspace* (RW) is the set of *reachable poses* of the robot.

III. Omniplus Designs

Because of current drone technology limitations (see section I), unidirectional thrusters have been selected for the design of our AWG. Optimal omniplus designs minimize the condition number of the wrench matrix $\mathbf{W}_t$ in order to equally share the efforts among the propellers for a given

desired wrench [6], [8], [7]. This property is interesting from a control point of view because it reduces the likelihood of saturating the actuators. Furthermore, the mechanical structure of omniplus designs allows for a simple allocation strategy implementation. For more in-depth information about omniplus designs, we refer the reader to [6]; from their work let us consider the following two definitions:

Definition 2: A multi-rotor design is a tuple $\mathscr{D} = (n, a, \mathbf{z}_{p_1}, \ldots, \mathbf{z}_{p_n}, \mathbf{GP}_1, \ldots, \mathbf{GP}_n)$ which describes the number of propellers n, their thrust coefficient a, their orientations and locations w.r.t. $\mathscr{F}_b$. We make the distinction between a *vectoring* part $\mathbf{Z} = (\mathbf{z}_{p_1}, \ldots, \mathbf{z}_{p_n})$, and an *etero-vectoring* part $\mathscr{P}_e = (n, a, \mathbf{GP}_1, \ldots, \mathbf{GP}_n)$.

Definition 3: Given $\underline{u} \geq 0$, a multi-rotor design $\mathscr{D}$ is omniplus ($O+$) if one of the following conditions holds:

$$\forall\, \mathbf{f} \in \mathbb{R}^6 \quad \exists\, \mathbf{u} \geq \underline{u}\mathbf{1} \quad \text{s.t.} \quad \mathbf{W}_t\mathbf{u} = \mathbf{f} \tag{8}$$

$$\text{rank}\,(\mathbf{W}_t) = 6 \quad \text{and} \quad \exists\, \mathbf{b} > \mathbf{0} \quad \text{s.t.} \quad \mathbf{W}_t\mathbf{b} = \mathbf{0} \tag{9}$$

where $\mathbf{1} \in \mathbb{R}^n$ is the column vector containing only ones.

A. Allocation Strategy

An allocation strategy that ensures the positiveness of the control inputs is needed because of the unidirectional thrusters. Given a desired wrench $\mathbf{f}_d \in \mathbb{R}^6$, Tognon et al. proves that the control input $\mathbf{u}^* = \mathbf{W}_t^\dagger \mathbf{f}_d$ always has at least a negative entry, where $\mathbf{W}_t^\dagger$ is the *Moore-Penrose* pseudoinverse of $\mathbf{W}_t$ [6]. Considering a positive vector $\mathbf{b}$ of the null space of $\mathbf{W}_t$ (which always exists by definition of omniplus design) we have $\mathbf{b} \perp \mathbf{u}^*$. Therefore $\mathbf{u}^{**} = \mathbf{u}^* + \lambda\mathbf{b}$ with $\lambda > 0 \in \mathbb{R}$ satisfies $\mathbf{f}_d = \mathbf{W}_t\mathbf{u}^{**}$. The goal of the allocation strategy is to find λ such that every element of $\mathbf{u}^{**}$ is greater or equal than $\underline{u}$ while minimizing the norm of $\mathbf{u}^{**}$. For more details we refer the reader to [6].

B. Balanced Omniplus Designs

An omniplus design is said *balanced*, if the vector $\mathbf{1}$ is in the null space of the wrench matrix i.e., $\mathbf{W}_t\mathbf{1} = \mathbf{0}$. Taking into account the allocation strategy presented previously, balanced omniplus designs allow for equally sharing the load among the propellers by having $\mathbf{b} = \mathbf{1}$, thus uniformly sharing the extra effort $\lambda\mathbf{b}$ among all the propellers.

C. Symmetry Study

Exploiting structural symmetries during the design process can be an advantage. Symmetries can simplify the mechanical design, the control of the system [5], and the optimization by reducing the search space [4]. For example, classical quadcopters naturally compensate for the drag effect of the propellers thanks to their symmetrical structure by a balanced rotational speed alternation. In this section we will study the impact of different types of symmetries from the point of view of balanced designs.

Let us consider a configuration with an even number of propellers n. A pair of propellers refers to both the i-th and the $i+\frac{n}{2}$-th propeller, with $i \in \left[1, \frac{n}{2}\right]$. We suppose that the propeller positions are fixed and symmetrically distributed around the perimeter of a circle of radius R, like in Fig. 2.

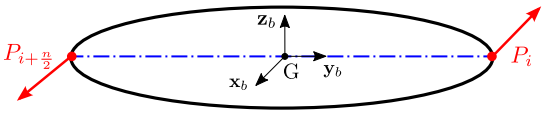

Fig. 2: Illustration of a pair of propellers.

Symmetry type	$\alpha_{i+\frac{n}{2}}$	$\beta_{i+\frac{n}{2}}$	$\mathbf{f}_T$
1	$-\alpha_i$	$-\beta_i$	$[f_x, f_y, f_z, 0, 0, 0]^T$
2	α_i	β_i	$[0, 0, f_z, 0, 0, m_z]^T$
3	α_i	$-\beta_i$	$[f_x, f_y, f_z, 0, 0, m_z]^T$
4	$-\alpha_i$	β_i	$[f_x, f_y, f_z, 0, 0, 0]^T$

TABLE I: Wrench applied to the structure by the propellers for different types of symmetries when $\mathbf{u} = \mathbf{1}$.

The orientation of the i-th propeller frame $\mathscr{F}_{p_i}$ w.r.t. the body frame $\mathscr{F}_b$ is determined by the Euler angles $(z-x-y)$: θ_i, α_i, β_i. The rotation matrix from $\mathscr{F}_b$ to $\mathscr{F}_{p_i}$ is noted $\mathbf{R}_{bp_i} \in SO(3)$. Since the positions of the propellers are fixed and symmetrically distributed, the parameter θ_i is known and we have $\theta_{i+\frac{n}{2}} = \theta_i + \pi$. Suppose that the orientation of the i-th propeller is fixed with $(\theta_i,\ \alpha_i,\ \beta_i)$. For a single pair of propellers (see Fig. 2), there exist four possible combinations of $\alpha_{i+\frac{n}{2}}$ and $\beta_{i+\frac{n}{2}}$ values to have a symmetrical structure: $\alpha_{i+\frac{n}{2}} = \pm\alpha_i$ and $\beta_{i+\frac{n}{2}} = \pm\beta_i$.

Let $t_i \in \mathbb{R}$ be the generated thrust and $\mathbf{f}_i \in \mathbb{R}^6$ the wrench applied at the CoM by the i-th propeller. For a given $(\theta_i,\ \alpha_i,\ \beta_i)$ we have:

$${}^b\mathbf{f}_i = \begin{pmatrix} t_i\left[\sin(\beta_i)\cos(\theta_i) + \cos(\beta_i)\sin(\alpha_i)\sin(\theta_i)\right] \\ t_i\left[\sin(\beta_i)\sin(\theta_i) - \cos(\beta_i)\sin(\alpha_i)\cos(\theta_i)\right] \\ t_i\cos(\alpha_i)\cos(\beta_i) \\ Rt_i\cos(\alpha_i)\cos(\beta_i)\sin(\theta_i) \\ -Rt_i\cos(\alpha_i)\cos(\beta_i)\cos(\theta_i) \\ -Rt_i\cos(\beta_i)\sin(\alpha_i) \end{pmatrix} \tag{10}$$

The total wrench $\mathbf{f}_T = \mathbf{f}_i + \mathbf{f}_{i+\frac{n}{2}} = [f_x, f_y, f_z, m_x, m_y, m_z]^T$ applied by a pair of propellers for the different symmetry types when all the propellers apply the same thrust of 1 N (i.e., $\mathbf{u} = \mathbf{1}$) is summarized in Table I. The second type of symmetry gives the best results if a balanced omniplus design is desired, almost all the components of the wrench $\mathbf{f}_T$ are naturally eliminated. Depending on the application, another symmetry might be more interesting. For instance, if the orientation of the AM is critical, symmetries 1 or 4 might be a better choice because the resulting moment applied to the platform is null.

IV. Design Optimization

A. Workspace Optimization

First, let us define a list $\boldsymbol{\theta} = (\alpha_1, \ldots, \alpha_n,\ \beta_1, \ldots, \beta_n)$ containing each propeller orientation[1], this list represents the vectoring part of a design $\mathscr{D}$. Considering the angles instead of the thrust direction allows for having a finer control over the final mechanical structure of the drone at the cost of making the optimization constraints nonlinear.

[1]We consider that $\alpha_i \in [0, 2\pi]$ and $\beta_i \in [\frac{-\pi}{2}, \frac{\pi}{2}]$.

Configurations	Angle	Propeller Index								$cond(\mathbf{W}_t)$	RW volume
		1	2	3	4	5	6	7	8		
Configuration 1	α_1	350.4	186.2	349.9	274.6	154.0	64.7	326.3	154.3		
	β_1	63.2	48.6	41.5	-0.1	18.3	14.4	51.3	40.5	4.942	1.559
Configuration 2	α_2	139.0	40.7	190.7	286.7	20.8	136.2	238.1	343.9		
	β_2	34.9	20.4	15.0	37.7	28.9	32.4	-10.2	11.9	4.942	0.938

TABLE II: Examples of two optimal omniplus configurations with similar matrix condition number but different RW volumes. The RW was computed with a spatial resolution of 10 cm over a rectangular volume of $8.64\,\mathrm{m}^3$.

Optimal omniplus designs minimize the condition number of the wrench matrix in order to equally share the load among the propellers. However, two optimal omniplus designs can result in different workspaces. An example of two configurations (with $n = 8$) with a similar wrench matrix conditioning but with different reachable workspaces (RWs) is presented in Table II. Minimizing the condition number of the wrench matrix does not take into account the elastic suspension, whereas the RW is directly limited by the spring force and torque. Faced with the problem complexity, a pure random search algorithm (see Algorithm 1) has been implemented to search for the design parameters that maximize the workspace. It generates N random optimal balanced omniplus designs and selects the one with the greatest workspace. The algorithm starts by generating a random vectoring part $\boldsymbol{\theta}$ with the function `randomAngles()`. Then the function `omniplusDesign()`, based on the algorithm presented in [6], outputs an optimal balanced omniplus design $\boldsymbol{\theta}_{O+}$. Next, the volume of the RW of the design $\boldsymbol{\theta}_{O+}$ with a nominal orientation (a null roll, pitch and yaw) is computed. Finally, the algorithm returns the configuration with the greatest RW volume.

Algorithm 1 Optimal dextAIR Design

Input: etero-vectoring part $\mathscr{P}_e$
Output: optimal propellers orientation $\boldsymbol{\theta}_{opt}$
1: $w_{opt} \leftarrow 0$
2: **for** $i = 0$ to N **do**
3: $\quad\boldsymbol{\theta}_{init} \leftarrow$ `randomAngles`(n)
4: $\quad\boldsymbol{\theta}_{o+} \leftarrow$ `omniplusDesign`$(\boldsymbol{\theta}_{init}, \mathscr{P}_e)$
5: $\quad w_{vol} \leftarrow$ `workspaceVolume`$(\boldsymbol{\theta}_{o+}, \mathscr{P}_e)$
6: $\quad$**if** $w_{vol} > w_{opt}$ **then**
7: $\quad\quad\boldsymbol{\theta}_{opt} \leftarrow \boldsymbol{\theta}_{o+}$
8: $\quad$**end if**
9: **end for**
10: **return** $\boldsymbol{\theta}_{opt}$

B. Optimization Results

1) Design Constraints: The spring anchoring point must be close to the CoM to limit the spring moment $\mathbf{N}_s$. Therefore a planar circular shape was considered for the structure. We suppose here that $G = A$, making $\mathbf{N}_s = \mathbf{0}$. The radius and the number of propellers are fixed respectively equal to 30 cm and $n = 8$. Only the orientation $\boldsymbol{\theta}$ of the propellers is optimized, their position is distributed symmetrically along the rotational axis of a circle every 45 deg.

2) Results: Two optimizations were carried out: (i) an unconstrained optimization where the propellers could take any orientation, (ii) an optimization where each β_i was constrained to $-25° \leq \beta_i \leq 90°$ in order to simplify the mechanical design. The results of the optimizations are available in Table III. They were carried out with a spatial resolution of 10 cm to compute the RW over a volume of $8.64\,\mathrm{m}^3$. The saturations of the actuators were chosen to be the same as the previous prototype [17] with a maximum thrust of 7.2 N. A thousand omniplus designs were generated ($N = 1000$) for both optimizations strategies. The optimization was conducted on a standard Dell laptop (Intel i5-2.5 GHz with 16 GiB of RAM) and took 25 min to complete.

The configuration with a constrained optimization problem reduces the workspace volume by 11 %. In addition, the new constraint makes the β_i angles converge to values close to zero (see Table III). To simplify the mechanics, the β_i angles are set to zero. The optimal angles of the constrained optimization are then similar to the angles of the SAM robot [7]. Therefore, for our prototype, the final configuration is the constrained α_i of Table III and $\beta_i = 0$ [deg]. The *final* configuration has a symmetry type 2 , which is the best one for a balanced omniplus design (see Section III-C).

C. Wrench-Feasible Workspace

The wrench-feasible workspace (WFW) is the set of poses that are wrench-feasible i.e., given any wrench $\mathbf{f}_d$ in a required set of wrenches $[\mathbf{f}]$, there exists a vector of propellers thrust $\mathbf{u} \in [\mathbf{u}]$ such that $\mathbf{W}_t\mathbf{u} = \mathbf{f}_d$ [18]. The WFW represents the workspace where the robot is useful for a particular defined task. It is an interesting performance index because it depends on the unidirectional saturation of the propellers. Hence, it is used here as an a posteriori verification to validate the results of the previous optimization.

A general analytical formulation of the WFW for CDPRs is presented in [18]. However, the analytical formulation is very complex for a 6-DoF robot. Consequently, efficient numerical methods were developed in order to compute the WFW of CDPRs using interval analysis [19]. In this work, the algorithm presented in [19] to compute the WFW of CDPRs was modified in order to compute the WFW of AMES using unidirectional thrusters. Below are the main differences regarding the computation of the WFW for the AMES w.r.t. a classical CDPR:

- It is better to project the equations in the body frame $\mathscr{F}_b$ so the expression of wrench matrix $\mathbf{W}_t$ does not depend on the pose of the robot, thus eliminating the *wrapping effect* [19] specific to interval analysis methods.

- The external wrench to consider in the analysis is now pose dependent. Indeed, the spring makes the external wrench on the AWG pose dependent, whereas with CDPRs the only external force is the constant gravity.

The INTLAB toolbox [20] was used in Matlab in order to compute the WFW of the robot. The WFW is computed considering the wrench norm generated by a load of 125 g placed at a distance of 19.5 cm from the CoM (gripper position in the prototype, see Fig. 4), so $[\mathbf{f}]$ is defined by forces of ± 1.25 N and moments of ± 0.24 N m. The WFW is computed for a constant nominal orientation (roll, pitch and yaw equal to zero) and a spatial resolution of 5 cm. The obtained WFW can be found in Fig. 3. The computed WFW has a volume of 1.6 m^3 which is equivalent to a sphere of radius 0.73 m. The obtained design is therefore able to manipulate small loads over a large workspace.

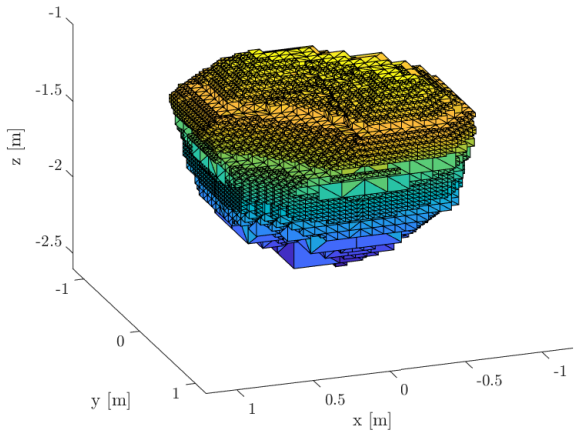

Fig. 3: WFW of the optimal structure. The colormap is only for visualization purposes, it has no physical meaning.

V. Experimental Setup

A. Mechanical Design

The prototype based on the geometrical parameters from the optimization was designed to be as light and as modular as possible. The two main materials used are carbon fiber and ABS. The robot has two main stages that can be seen in Fig. 4. The structure of the lower stage is made with several carbon fiber tubes so that different modules can be easily attached to it using 3D printed parts. The upper stage contains the heaviest components to raise the CoM so that it comes closer to the spring anchoring point. The propellers used are the GEMFAN-51499, and the rotors are X-NOVA Lightning V2N 2208-1700Kv.

B. Electronics

The robot has two *GOKU HD GN745 EVO* flight controllers (FC) with embedded ESCs and inertial measurement units to simplify the cabling. They run a modified version of the betaflight firmware `https://betaflight.com/`

Fig. 4: New dextAIR prototype.

known in the drone FPV (First Person View) community. The firmware is modified in order to implement a closed loop regulation of the propellers velocities. The implemented controller is a discrete anti-wind-up PI (proportional-integral) running at 8 kHz. The source code of the modified firmware is available at `https://github.com/jacqu/betalink`.

The robot has two 1400 mAh 6S lithium polymer battery packs, one for each FC. Another 2300 mAh 3S lithium polymer battery pack is used to power an on-board CPU (NVIDIA Jetson Xavier NX). The on-board computer handles the AWG control algorithms and communicates with a ground station through Wi-fi TCP/IP sockets thanks to the open-source Simulink toolbox RPIt developed in our lab [21]. The on-board computer communicates with the two FCs by USB.

The pose of the AWG is acquired by a Vicon Bonita motion-capture system measuring the 6-DoF pose vector of the AWG with a refresh rate of 240 Hz.

C. Control Law

In order to follow a reference trajectory $\mathbf{X}_{ref} = (\mathbf{p}_{ref}^T \; \boldsymbol{\eta}_{ref}{}^T)^T$, the same computed torque control law proposed in [17] is used to compute the reference wrench $\mathbf{f}_{ref}$:

$$\mathbf{f}_{ref} = \hat{\mathbf{W}}_{\mathbf{t}}^{-1} \left(\hat{\mathbf{M}} \left(\ddot{\mathbf{X}}_{ref} + \mathbf{K}_p \mathbf{e} + \mathbf{K}_d \dot{\mathbf{e}} + \mathbf{K}_i \int \mathbf{e} \right) + \hat{\mathbf{C}} \dot{\mathbf{X}} + \hat{\mathbf{G}} \right) \quad (11)$$

where $\mathbf{K}_p, \mathbf{K}_i, \mathbf{K}_d \in \mathbb{R}^{6\times 6}$ are positive definite diagonal matrices, and $\mathbf{e} = \mathbf{X}_{ref} - \mathbf{X}$ the pose error. The matrices $\hat{\mathbf{M}}$, $\hat{\mathbf{C}}$, $\hat{\mathbf{G}}$ and $\hat{\mathbf{W}}_{\mathbf{t}}$ are the estimates of the model parameters of (3). Finally, the allocation strategy explained previously (see Section III-A) is used to convert the desired wrench $\mathbf{f}_{ref}$ on the robot in propeller thrusts.

VI. Preliminary Experimental Tests

The computed torque controller is embedded and runs at a frequency of 200 Hz. The model parameters used to tune the controller are summarized in Table IV.

A. Trajectory Tracking

In this test, the robot follows a 6-DoF polynomial trajectory. The values used for the controller are the following: $\mathbf{K}_p = 90.\mathbf{I}_6$, $\mathbf{K}_i = 300.\mathbf{I}_6$, $\mathbf{K}_d = 20.\mathbf{I}_6$. A video of the trajectory tracking is attached to this paper (`https://www.youtube.com/watch?v=DPVq50Pw3yg`). The results of the trajectory tracking and the control inputs can

Configurations	Angles	Propeller Index								$cond(\mathbf{W}_t)$	RW volume
		1	2	3	4	5	6	7	8		
Unconstrained	α_i	45.7	125.2	44.7	-177.8	-45.2	-125.3	-44.3	179.5		
	β_i	-34.4	1.0	35.6	54.7	34.9	-0.6	-36.1	-54.7	4.714	2.636
Constrained	α_i	54.3	125.0	-125.6	-55.1	54.4	124.8	-125.7	-55.1		
	β_i	-0.5	-0.5	0.5	0.5	-0.5	-0.5	0.6	0.6	4.714	2.348

TABLE III: Optimization results for the unconstrained and constrained optimization problems. The angles are given in the $[-180°, 180°]$ interval to highlight structural symmetries.

Parameter	Description	Value	Unit
k	Spring stiffness	22	$[\mathrm{N\,m^{-1}}]$
l_0	Spring free length	0.78	[m]
m	Total mass	2.717	[kg]
I_{xx}	Inertia moment about $\mathbf{x}_b$	35.9×10^{-3}	$[\mathrm{kg\,m^2}]$
I_{yy}	Inertia moment about $\mathbf{y}_b$	35.9×10^{-3}	$[\mathrm{kg\,m^2}]$
I_{zz}	Inertia moment about $\mathbf{z}_b$	71.8×10^{-3}	$[\mathrm{kg\,m^2}]$
a	Thrust coefficient	1.82×10^{-6}	$[\mathrm{N\,rad^{-2}\,s^2}]$
$\mathbf{GP}_i$	Propellers and CoM distance	0.3	[m]

TABLE IV: Model parameters.

Axis	x	y	z	roll	pitch	yaw
RMS [mm or deg]	0.4	0.3	1.6	0.7	0.5	0.3

TABLE V: Trajectory tracking RMS error per DoF.

be found in Fig. 5. The robot presents a good accuracy with a maximum root-mean-square (RMS) error of 1.6 mm for the position and 0.7° for the orientation (see Table V).

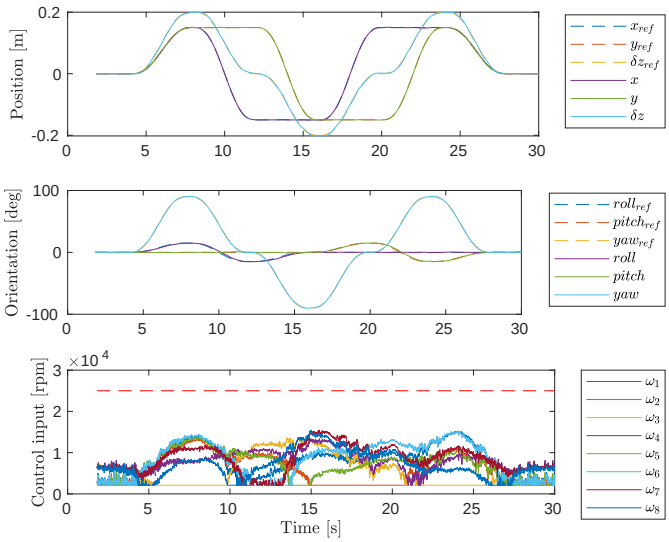

Fig. 5: Trajectory tracking and control input. Actuators saturation is represented by the red dashed line.

B. Reachable Workspace Characterization

In Fig. 6, the theoretical RW of the optimal structure is computed with the new propulsion units. Some real positions reached by the new prototype are also depicted in order to experimentally test the boundaries of the RW. The boundaries of the reachable workspace along $\mathbf{x}_f$ and $\mathbf{y}_f$ around the equilibrium point are tested. The boundaries of the RW along $\mathbf{z}_f$ cannot be tested with our experimental setup because the AWG would collide with the ground or the roof.

The new prototype has a RW volume of 5.63 $\mathrm{m^3}$ whereas the previous prototype had a RW volume of 0.51 $\mathrm{m^3}$. However, if the RW of the new prototype is computed with the actuator saturations of the previous prototype (maximum thrust of 7.2 N) the volume becomes 2.38 $\mathrm{m^3}$. Therefore, the workspace improvement is not only due to the thrust increase but also to the new design.

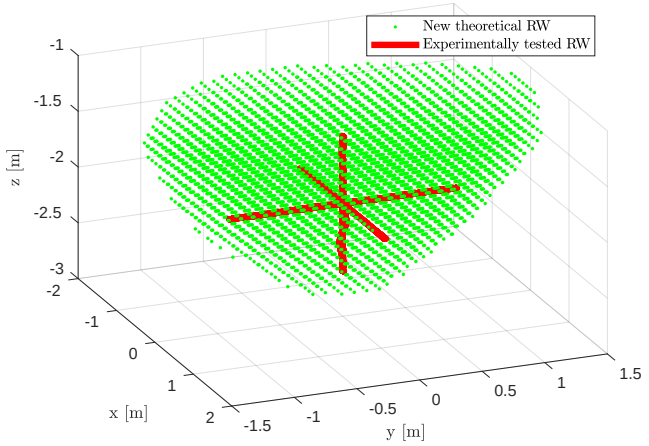

Fig. 6: Experimental reachable workspace characterization.

VII. Conclusion and Perspectives

In this paper, criteria and techniques from the CDPR and AM community were adapted to design, evaluate and study the performances of an Aerial Manipulator with Elastic Suspension using unidirectional thrusters. An algorithm to optimally design an AMES is proposed. The algorithm maximizes the RW of the system and ensures to have a balanced omniplus AWG. The optimization results are used to build a prototype whose RW boundaries are tested experimentally. The new RW volume is increased by almost ten times when compared with the older one.

Future work will focus on embedding the vision system inside the AWG in order to control the robot without a motion capture system. Furthermore, advanced optimal control strategies will be implemented in order to have an optimal allocation strategy and exploit the system redundancy.

Acknowledgments

The authors thank Jean Soudier and Mandela Ouafo for their help during the development of the prototype.

REFERENCES

[1] M. Tognon, H. A. T. Chávez, E. Gasparin, Q. Sablé, D. Bicego, A. Mallet, M. Lany, G. Santi, B. Revaz, J. Cortés, and A. Franchi, "A Truly-Redundant Aerial Manipulator System With Application to Push-and-Slide Inspection in Industrial Plants," *IEEE Robotics and Automation Letters*, vol. 4, no. 2, pp. 1846–1851, Apr. 2019.

[2] K. Bodie, M. Brunner, M. Pantic, S. Walser, P. Pfndler, U. Angst, R. Siegwart, and J. Nieto, "An Omnidirectional Aerial Manipulation Platform for Contact-Based Inspection," in *Robotics: Science and Systems XV*. Robotics: Science and Systems Foundation, Jun. 2019.

[3] R. Rashad, J. Goerres, R. Aarts, J. B. C. Engelen, and S. Stramigioli, "Fully Actuated Multirotor UAVs: A Literature Review," *IEEE Robotics Automation Magazine*, vol. 27, no. 3, pp. 97–107, Sep. 2020.

[4] S. Park, J. Lee, J. Ahn, M. Kim, J. Her, G.-H. Yang, and D. Lee, "ODAR: Aerial Manipulation Platform Enabling Omnidirectional Wrench Generation," *IEEE/ASME Transactions on Mechatronics*, vol. 23, no. 4, pp. 1907–1918, Aug. 2018.

[5] D. Brescianini and R. D'Andrea, "An omni-directional multirotor vehicle," *Mechatronics*, vol. 55, pp. 76–93, Nov. 2018.

[6] M. Tognon and A. Franchi, "Omnidirectional Aerial Vehicles With Unidirectional Thrusters: Theory, Optimal Design, and Control," *IEEE Robotics and Automation Letters*, vol. 3, no. 3, pp. 2277–2282, Jul. 2018.

[7] Y. S. Sarkisov, M. J. Kim, D. Bicego, D. Tsetserukou, C. Ott, A. Franchi, and K. Kondak, "Development of SAM: Cable-Suspended Aerial Manipulator," in *2019 International Conference on Robotics and Automation (ICRA)*, May 2019, pp. 5323–5329.

[8] M. Hamandi, K. Sawant, M. Tognon, and A. Franchi, "Omni-Plus-Seven (O7+): An Omnidirectional Aerial Prototype with a Minimal Number of Unidirectional Thrusters," in *2020 International Conference on Unmanned Aircraft Systems (ICUAS)*, Sep. 2020, pp. 754–761.

[9] R. Kurtz and V. Hayward, "Dexterity measures with unilateral actuation constraints: The n+1 case," *Advanced Robotics*, vol. 9, no. 5, pp. 561–577, Jan. 1994.

[10] J. Eden, D. Lau, Y. Tan, and D. Oetomo, "Unilateral Manipulability Quality Indices: Generalized Manipulability Measures for Unilaterally Actuated Robots," *Journal of Mechanical Design*, vol. 141, no. 9, Jul. 2019.

[11] S. Tadokoro, S. Nishioka, T. Kimura, M. Hattori, T. Takamori, and K. Maeda, "On fundamental design of wire configurations of wire-driven parallel manipulators with redundancy: Proceedings of the 1996 Japan-USA Symposium on Flexible Automation. Part 2 (of 2)," in *Proceedings of the Japan/USA Symposium on Flexible Automation*, ser. Proceedings of the Japan/USA Symposium on Flexible Automation, K. Stelson and F. Oba, Eds., Dec. 1996, pp. 151–158.

[12] T. Bruckmann, L. Mikelsons, and M. Hiller, "A Design-To-Task Approach for Wire Robots," in *Interdisciplinary Applications of Kinematics*, A. Kecskeméthy, V. Potkonjak, and A. Müller, Eds. Dordrecht: Springer Netherlands, 2012, pp. 83–97.

[13] S. Abdolshah, D. Zanotto, G. Rosati, and S. K. Agrawal, "Optimizing Stiffness and Dexterity of Planar Adaptive Cable-Driven Parallel Robots," *Journal of Mechanisms and Robotics*, vol. 9, no. 3, p. 031004, Jun. 2017.

[14] H. Hussein, J. C. Santos, J.-B. Izard, and M. Gouttefarde, "Smallest Maximum Cable Tension Determination for Cable-Driven Parallel Robots," *IEEE Transactions on Robotics*, pp. 1–20, 2020.

[15] A. Alamdari, M. Anson, and V. Krovi, "Orientation Workspace and Stiffness Optimization of Cable-Driven Parallel Manipulators With Base Mobility," *Journal of Mechanisms and Robotics*, vol. 9, Jan. 2017.

[16] F. Hao and J. P. Merlet, "Multi-criteria optimal design of parallel manipulators based on interval analysis," *Mechanism and Machine Theory*, vol. 40, no. 2, pp. 157–171, Feb. 2005.

[17] A. Yiğit, M. A. Perozo, L. Cuvillon, S. Durand, and J. Gangloff, "Novel Omnidirectional Aerial Manipulator With Elastic Suspension: Dynamic Control and Experimental Performance Assessment," *IEEE Robotics and Automation Letters*, vol. 6, no. 2, pp. 612–619, Apr. 2021.

[18] P. Bosscher, A. T. Riechel, and I. Ebert-Uphoff, "Wrench-feasible workspace generation for cable-driven robots," *IEEE Transactions on Robotics*, vol. 22, no. 5, pp. 890–902, Oct. 2006.

[19] M. Gouttefarde, D. Daney, and J. Merlet, "Interval-Analysis-Based Determination of the Wrench-Feasible Workspace of Parallel Cable-Driven Robots," *IEEE Transactions on Robotics*, vol. 27, no. 1, pp. 1–13, Feb. 2011.

[20] S. Rump, "INTLAB - INTerval LABoratory," in *Developments in Reliable Computing*, T. Csendes, Ed. Dordrecht: Kluwer Academic Publishers, 1999, pp. 77–104, http://www.tuhh.de/ti3/rump/.

[21] J. Gangloff, A. Yiğit, and M. Lesellier, "RPIt," 2020. [Online]. Available: https://github.com/jacqu/RPIt/